Journal of Physics: Conference Series **488** (2014) 012015 doi:10.1088/1742-6596/488/1/012015

Experimental strategies for optical pump – soft x-ray probe experiments at the LCLS

B K McFarland[1], **N Berrah**[2] ,**C Bostedt**[3], **J Bozek**[3], **P H Bucksbaum**[1,4], **J C Castagna**[3], **R N Coffee**[3], **J P Cryan**[1,4], **L Fang**[2], **J P Farrell**[1,4], **R Feifel**[5], **K J Gaffney**[1], **J M Glownia**[1,4], **T J Martinez**[1,6], **S Miyabe**[1],**M Mucke**[5], **B Murphy**[2], **A Natan**[1], **T Osipov**[2] , **V S Petrović**[1,4], **S Schorb**[3], **Th Schultz**[7], **L S Spector**[1,4], **M Swiggers**[3], **F Tarantelli**[8], **I Tenney**[1,4], **S Wang**[1,4], **J L White**[1,4], **W White**[3], and **M Gühr**[1*]

[1] PULSE Institute, SLAC National Accelerator Laboratory, Menlo Park, CA 94025, USA
[2] Physics Department, Western Michigan University, Kalamazoo, MI 49008, USA
[3] LCLS, SLAC National Accelerator Laboratory, Menlo Park, CA 94025, USA
[4] Departments of Physics and Applied Physics, Stanford University, Stanford, CA 94305, USA
[5] Department of Physics and Astronomy, Uppsala University, Uppsala, Sweden
[6] Department of Chemistry, Stanford University, Stanford, CA 94305, USA
[7] Max-Born-Institut, 12489 Berlin, Germany
[8] Dipartimento di Chimica, Universita di Perugia, and ISTM-CNR, 06123 Perugia, Italy

*E-mail: mguehr@stanford.edu

Abstract. Free electron laser (FEL) based x-ray sources show great promise for use in ultrafast molecular studies due to the short pulse durations and site/element sensitivity in this spectral range. However, the self amplified spontaneous emission (SASE) process mostly used in FELs is intrinsically noisy resulting in highly fluctuating beam parameters. Additionally timing synchronization of optical and FEL sources adds delay jitter in pump-probe experiments. We show how we mitigate the effects of source noise for the case of ultrafast molecular spectroscopy of the nucleobase thymine. Using binning and resorting techniques allows us to increase time and spectral resolution. In addition, choosing observables independent of noisy beam parameters enhances the signal fidelity.

1. Introduction

Molecules exhibit the ability to transform light energy into chemical [1], electrical [2], or thermal energy [3] with very high selectivity and efficiency. Initially, absorbed light energy is stored in rearranged valence electrons, leading to altered intramolecular forces and subsequent nuclear motion on an ultrafast timescale. The topology of the photoexcited molecular potential energy surface (PES) determines the efficiency for light energy conversion and contains regions in which the Born-

Oppenheimer approximation (BOA) breaks down [4, 5]. The theoretical treatment of non-BOA processes is most accurate for isolated quantum systems, eliminating the complications of additional solvent coordinates. Thus, gas phase experiments, in combination with advanced theoretical modeling, are valuable for understanding light energy conversion.

Ultrafast experiments are typically implemented in the pump-probe fashion; a pump pulse first excites the molecule, thereby launching a nuclear wavepacket on a PES. A probe pulse with a variable time delay then interrogates the photoinduced dynamics. In gas phase experiments, the probe pulse typically ionizes the molecule yielding mass resolved photoions [6] or energy resolved photoelectrons detected as a function of pump-probe delay [7]. Due to the wide availability of ultrafast lasers in the optical frequency domain, most of these experiments are carried out in the infrared, visible, or ultraviolet regions.

Probing photoinduced molecular dynamics with ultrashort x-ray pulses complements optical probing with additional opportunities. In particular X-rays offer element/site selectivity. X-rays interact with core electron wavefunctions which are highly localized, and their binding energies are determined by element and position inside the molecule. The photoelectron induced after core ionization thus emerges from a locality in the molecule and the so called chemical shift contains local information about chemical bonding [8]. X-ray fluorescence and Auger decay of core holes also contain the core hole wavefunction in the dipole or Coulomb matrix element. This leads to high spatial and element sensitivity on the valence electrons.Ultrafast x-ray sources have become available at synchrotrons [9] however with rather limited single pulse energy, making the gas phase photoionization method hard if not impossible. Recently, x-ray free electron lasers (FELs) provide milliJoule level x-ray pulses [10-12] suitable for photoion and photoelectron probe techniques, and even nonlinear experiments in gas phase targets [13-17]. X-ray FELs usually operate by self amplified spontaneous emission (SASE) of an electron bunch at the beginning of the undulator resulting in large spectral, pulse energy and pulse length fluctuations from pulse to pulse [18]. Using an independent optical laser for photoexcitation introduces additional variation due to laser/X-ray delay fluctuations which occur despite locking the electron gun laser to the optical excitation laser. If the desired spectral or temporal resolution in the experiment is smaller than the instrument jitter, important features are lost in averaged or transient spectra.

This paper describes the experimental setup and important data analysis strategies of an ultraviolet (UV) pump – soft x-ray probe experiment on the nucleobase thymine. All nucleobases show interesting excxited state photodynamics. After UV excitation with giant cross sections as high as 30Mbarn, the excited state population is funneled into lower lying electronic states on an ultrafast timescale. This mechanism, already manifest in single molecules, is responsible for protecting the nucleobases inside DNA and RNA from light induced damage processes [19-21].

The experiment was performed in September 2011 at the linac coherent light source (LCLS). We demonstrate how to select and resort observables in an optical pump-x-ray probe experiment to compensate for SASE fluctuations with the aim to increase spectral and temporal fidelity. This can be achieved in two ways. First, by selecting molecular observables that are independent of fluctuating laser/X-ray parameters. Photoelectrons will show a kinetic energy modulation following the X-ray pulse spectral jitter. In constrast, Auger or fluorescence decay yields and energies do not shift with photon energy and are thus easy to interpret. Second, by single shot detection of jittering machine parameters and subsequent binning and resorting of data to enhance contrast. We illustrate this below with examples of X-ray/laser delay and photon energy resorting.

2. Experiment

We performed our experiments at the AMO scientific instrument of LCLS at SLAC National Accelerator Laboratory [22]. A schematic overview is given in figure 1. Molecules in the interaction region were excited with an ultrashort UV pump pulse (~70 fs pulse duration, hν=4.5 eV) produced by third harmonic generation of a commercial Ti:Sapphire amplified laser. The molecular dynamics after photoexcitation was probed by a soft x-ray pulse (<70 fs pulse duration). Its photon energy was ~ 25

eV above the oxygen K edge, leading to core ionization. We used a magnetic bottle electron spectrometer to detect the Auger decay of the oxygen core holes from 480 eV to 520 eV and additionally the valence photoelectron spectrum at even higher kinetic energies [13,14,19]. A retarding field of 470 V was applied to the electrons to optimize energy resolution in the Auger region, while compromising resolution for valence photoemission.

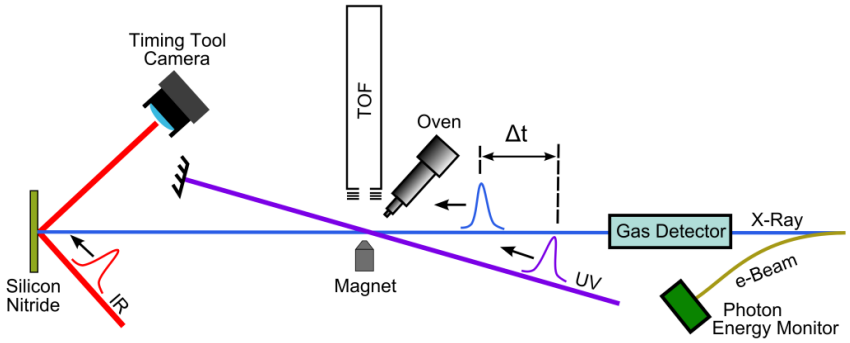

Figure 1. Setup at the AMO scientific instrument of the LCLS. UV pump and soft x-ray probe pulses have a delay Δt and excite/interrogate the molecular dynamics. Molecules are delivered by an evaporative source described in detail in figure 2. X-ray pulse energy (acquired from a gas detector), photon energy, and relative delay as well as the electrons yielded by the FEL pulses are recorded on every shot.

The molecules, available as a low vapor pressure powder (Sigma Aldrich, purity >99%), were introduced into the interaction region by an evaporative source, heated to about 420 K. The source shown in figure 2 was designed specifically for this experiment and we will explain its features and design more extensively here. The oven produces a narrow and continuous gas beam for samples with low vapor pressure, by evaporating the molecules and directing them through a thin capillary towards the interaction region. Compared to actuated valves, this source contains no moving parts requiring maintenance. Our capillary-oven provides a narrower beam compared to a simple Knudsen cell with a hole in the heated reservoir. A continuous source generally gives rise to higher pump loading compared to actuated valves. Molecules with low vapor pressure at room temperature and a high sticking coefficient do not impose that problem. We provided a liquid nitrogen cooled surface opposite to the oven for preferential condensation of the sample.

The molecular source consists of three main parts. A body machined out of a 1” Al rod contains the sample powder. The body has an inner rim, which avoids sample falling into capillary when the oven is mounted with the capillary tip pointing down. An Al cap seals the oven by a tapered thread painted with graphite. The oven tip is made out of an Al capillary which is press fitted into an Al screw (1/4”-20 thread painted with graphite), and attached to the body. The capillary itself has an inner diameter of 0.9 mm, outer diameter of 1.6 mm and a typical length of 40-50 mm. The capillary is too fragile for a simple press fit into the screw. We therefore drilled a hole into the Al screw which was slightly larger than the capillary. We subsequently filled the capillary with water and dipped the assembly of screw and capillary into liquid nitrogen. The freezing water expanded the capillary tight into the Al screw. The body, cap, and capillary assembly of the oven are separately heated by kapton sheet heating elements (Omega), providing up to 30W heating power. The sheet heaters are attached to the oven by Al sheet metal covers. To provide good thermal contact to the capillary, we designed a capillary casing that clamped to the capillary. During experiments, the tip is kept a few Kelvin higher than the rest of the oven to avoid accumulation of sample inside the capillary. The temperatures of all three parts of the oven can be independently monitored by thermocouples.

We tested the oven for jet divergence and sample density out of the capillary of 47 mm. The spread was determined by evaluating the spot size of condensed sample on a glass plate. The total mass flux out of oven was determined by deposition on a cooled quartz crystal monitor. Table 1 presents the oven parameters for three different evaporation temperatures. It is well documented that the thymine molecules do not suffer thermally induced fragmentation in this temperature range [23,24].

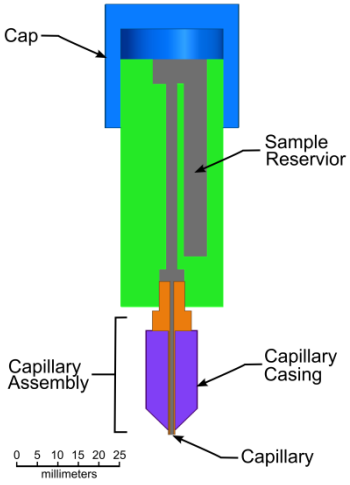

Figure 2. Oven assembly. The oven consists of three parts: the cap, the body (with sample reservoir) and the capillary assembly. All three parts can be separately heated by sheet heaters attached to the surface of each element.

Table 1. Thymine molecular source characteristics for three different temperatures. The vapour pressure of thymine is taken from reference [25]. The divergence was measured by deposition on a substrate. The full width half maximum (FWHM) of the spot density profile reflects the angular width of the molecular source. The mass rate was evaluated a quartz crystal balance. The sample density at the exit of the capillary is estimated from mass rate and molecular thermal velocity. The oven has now also been successfully used for uracil and aminophenol.

Temperature (K)	Thymine vapor pressure (mbar)	Angular FWHM (deg)	Mass rate (ng/sec)	Sample density ($1/cm^3$)
408	$4x10^{-4}$	10	3.4	10^{11}
428	$2.5x10^{-3}$	16	100	$2x10^{12}$
448	$1.4x10^{-2}$	40	700	$1.7x10^{13}$

The experimental setup at LCLS contains single shot diagnostics for essential parameters like x-ray central wavelength, pulse energies of optical and x-ray pulses, and relative delay between optical and x-ray pulses [26]. The single shot x-ray spectral monitor determines the center wavelength of x-rays from electron energy loss after undulator passage. The x-ray pulse energy monitors are based on nitrogen gas cells which are crossed by the x-ray beam. The x-ray induced core ionization and its relaxation processes result in UV photoluminescence, which is recorded on every shot [27]. The single shot optical pulse – x-ray delay monitor is documented in [28]. The x-ray pulse hits Si_3N_4 film on a Si substrate under normal incidence, thereby changing the reflectivity of sample. An infrared pulse is reflected from the Si_3N_4 film under a large angle. The transient reflectivity change is thereby encoded in the spatial profile of the reflected infrared pulse. The infrared pulse has a stable delay with respect to the UV pump pulse. The magnetic bottle time of flight spectrometer used in the experiment has a

2m long flight tube and uses a combination of a permanent magnet and a solenoid to shape the magnetic field with optimal collection efficiency [13,14,19]. The magnetic bottle has a small spatial region for optimal collection of electrons, which we overlapped with the optical/x-ray pulse interaction region. We typically detected tens of electron hits on the multichannel plate detector at the end of the flight tube. Since we have pulse pile up in certain regions we cannot distinguish individual electron hits. However, the single shot electron yield is not high enough to determine a complete spectrum and many shots are typically added for this purpose.

3. Results and Discussion

The single shot parameters are recorded at the repetition rate of the free electron laser, which currently is 120 Hz. Each parameter is saved as a time series in large data files. Before resorting and binning according to experimental parameters we check if the time series of the different parameters match up. Due to detector or data storage errors a shot can be skipped in one parameter set without being skipped in others. This slippage will lead to erroneous results in single shot binning and resorting algorithms. One way to evaluate the integrity of the parameter time series is checking correlations. For instance, the total amount of detected electrons must be correlated to the x-ray pulse energy.

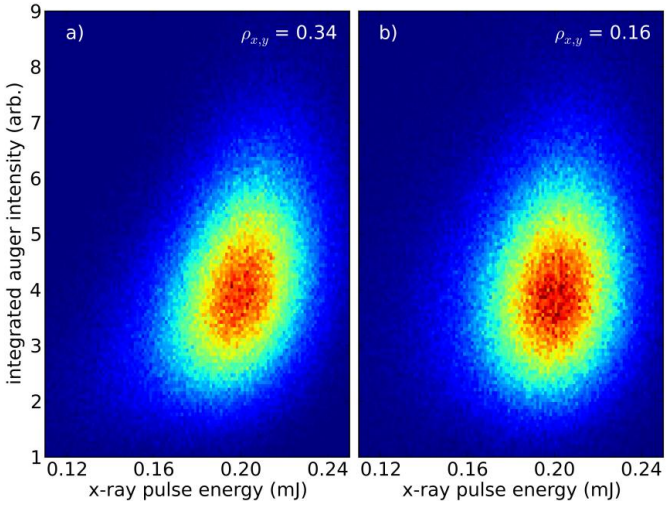

Figure 3. Correlation of integrated magnetic bottle spectrometer signal with x-ray pulse energy. a) Ordering of the time series as recorded. The Pearson correlation coefficient $\rho_{x,y}$ is 0.34. b) One of the two time series permuted by one shot. The correlation coefficient decreases to 0.16, indicating less correlation between the parameters.

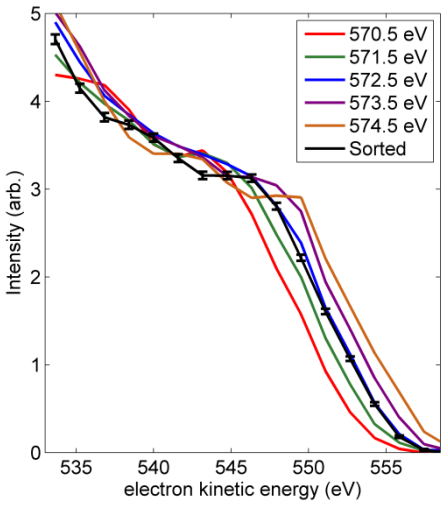

Figure 4. Binning and resorting thymine valence photoelectron spectra according to photon energy. The spectra are given as a function of kinetic energy and grouped according to photon energy into 1eV wide bins centered at the values listed in the legend (colored). The black curve is corrected for photon energy jitter. The binned spectra show a clear offset in the spectral step reflecting the bin photon energy.

Figure 3 shows the correlation plot of integrated magnetic bottle spectrometer signal vs. x-ray pulse energy. The ordering recorded in the experiment is shown in (a) and the order of one time series permuted by 1 shot is used in (b). The slope in the correlation plot in (a) indicates that the two observables are correlated; we evaluate a Pearson correlation coefficient of 0.34. The correlation plot of the permuted data set in (b) shows a coefficient of 0.16, less than in (a). Systematic variation of the shot permutation leads to a maximum in the correlation coefficient for case (a). Thus we deduce that the original time-ordering as in (a) is correct. The fact that the correlation coefficient in (b) is still

different from zero (uncorrelated case) is related to the noise spectrum of the variables. The pulse energy of two adjacent shots of the free electron laser show some correlation. If the first pulse was high in energy, the second one also tends to be high. This translates to a non-vanishing correlation between the magnetic bottle electron spectrometer yield and pulse energy even for the permuted case. Since the slippage of single shots can occur at any point in the data series, the correlation should ideally be checked for various subsets of the parameter arrays.

Figure 4 demonstrates the binning and resorting method with the example of valence photoemission. As mentioned above, the kinetic energy of the valence photoelectrons is dependent on the photon energy. Thus, the kinetic energy changes from shot to shot as the photon energy changes. The colored lines in figure 4 present valence photoelectron spectra of thymine binned into different photon energy intervals. In order to obtain these data, the electron time of flight (TOF) spectrum was saved for every shot together with the measured x-ray photon energy. We then sorted all shots in 1eV wide bins and accumulated the spectral information for these bins. The center of the photon energy interval is given in the legend. The spectra of different bins are clearly shifted by the bin size of 1 eV. The black curve represents the spectra corrected for the photon energy jitter. The resolution is poor compared to literature data [29]. The spectrometer was optimized with a retarding potential for the Auger decay region. In the valence region, the energy resolution is only about 4eV due to the shorter flight time and the valence structure is washed out. Moreover, the apparent binding energy is shifted by approximately 10 eV. Since we have not calibrated the photon energy detector, the 10eV inaccuracy is likely to result from an inaccurate detector reading.

The individually binned datasets in figure 4 are normalized to the number of laser shots falling into the photon energy bin. Nevertheless they show a systematic trend in the signal strength. The initial spectral rise for higher photon energy bins is lower compared to the low photon energy bins. This indicates that an additional parameter is correlated with the photon energy. Figure 5 shows the correlation plot of soft x-ray photon energy and pulse energy. We clearly observe an anti-correlation between photon energy and pulse energy as indicated by the negative slope of the distribution. This example points out that binning and resorting can exhibit systematic trends if the resorting parameter is correlated (or anti-correlated) with other parameters influencing the signal. For future experiments on photoelectron spectroscopy, this has important consequences. When binning data according to photon energy, the systematic change in pulse energy has to be taken into account. As long as the photoelectron signal is linear, as in our case, one can rescale the signal in each photon energy bin according to the pulse energy. To create the resorted spectrum (black) in figure 4, we normalized on the pulse energy. Nonlinear experiments however will most likely require an additional filtering on pulse energy instead of rescaling.

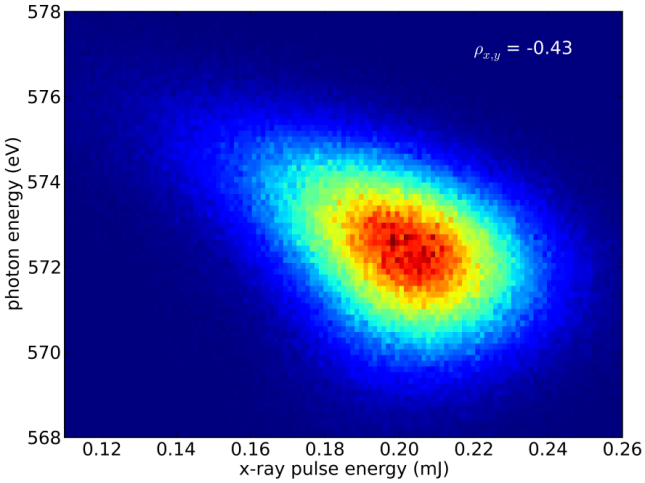

Figure 5. Correlation of photon energy with x-ray pulse energy. The dataset are anti-correlated with a correlation coefficient $\rho_{x,y}$ = -0.43.

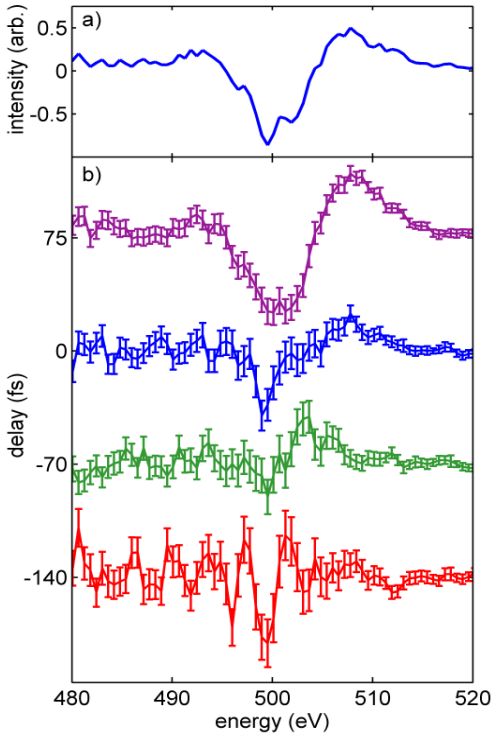

Figure 6. Auger difference spectra (UV on – UV off). a) All data from a particular dataset, no binning. b) Data binned on the single shot delay monitor for -140 to 75 fs time delay between UV pump and soft x-ray probe pulse. We clearly observe structures growing in the difference spectra after zero time delay.

In addition to binning and resorting, we can choose molecular observables that are independent of fluctuating parameters. We demonstrated in figure 4 that valence photoelectrons are sensitive to the x-ray photon energy jitter. The normal (non-resonant) Auger electron energy, however, is insensitive to this fluctuating parameter. Therefore, we chose to optimize the resolution of the magnetic bottle spectrometer in the region containing normal Auger features associated with oxygen 1s ionization.

Figure 6 shows spectra in the energy range of oxygen core-hole Auger decay. We present Auger difference spectra between UV excited and unexcited molecules. Figure 6 a) shows one complete dataset, which is clearly modulated with a positive difference signal at 507 eV and negative difference signal around 500 eV. While recording these data, the single shot delay monitor [28] was used to log the relative delay between the UV excitation and soft x-ray probe pulse. The UV excited Auger spectra were corrected for the single shot delay jitter. The unexcited molecular Auger spectra were subtracted. The result is shown in Figure 6 b) in 4 different delay bins ranging from -140 to 75 fs pump-probe delay. The nominal jitter of the delay was larger than 250 fs and the onset of features from zero to 75 fs delay clearly shows the improvement of time resolution due to the delay monitor. The signal to noise ratio increases towards larger delays since more shots fall into these bins. The spectral features in the difference spectra are the subject of a separate publication [30]. In short, we observe the population the ultraviolet excited electronic state of thymine.

In summary, we have shown the important experimental ingredients of our UV pump – LCLS soft x-ray probe experiment on the photoexcited dynamics of thymine. The molecular source designed for this purpose shows narrow divergence and high molecular density. We show how the correct time ordering of parameters can be checked using correlation. Furthermore, we describe how we bin and resort valence photoemission spectra and demonstrate that correlated parameters systematically shape the data. The Auger decay spectra are not sensitive to photon energy jitter. For this case, we show that time reordering using a single shot delay detector allows us to obtain time resolution exceeding the delay jitter.

This work was supported by the AMOS program within the Chemical Sciences, Geosciences, and Biosciences Division of the Office of Basic Energy Sciences, Office of Science, U.S. Department of Energy. M. G. acknowledges funding via the Office of Science Early Career Research Program through the Office of Basic Energy Sciences, U.S. Department of Energy. R. F. thanks the Swedish Research Council, the Göran Gustafsson Foundation (UU/KTH), and the Knut and Alice Wallenberg Foundation, Sweden for financial support. The experimental research was carried out at the Linac Coherent Light Source (LCLS) at the SLAC National Accelerator Laboratory. LCLS is an Office of Science User Facility operated for the U.S. Department of Energy Office of Science by Stanford University. We thank Mike Bogan for lending us a quartz crystal monitor.

References

[1] Polli D *et al.* 2010 *Nature* **467** 440
[2] Gratzel M 2005 *Inorganic Chem.* **44** 6841
[3] Crespo-Hernandez C E, Cohen B, Hare P M, and Kohler B 2004 *Chem. Rev.* **104** 1977
[4] Domcke W, Yarkony D, and Koeppel H (eds) 2004 *Conical Intersections* (Singapore: World Scientific)
[5] Levine B G, Martinez T J 2007 *Ann. Rev. Phys. Chem.* **58** 613
[6] Kotur M, Weinacht T C, Zhou C, and Matsika S 2011, *Phys. Rev. X* **1** 021010
[7] Stolow A, Bragg A E, and Neumark D M 2004 *Chem. Rev.* **104**, 1719
[8] Siegbahn K 1969 *ESCA applied to free molecules* (New York: North Holland)
[9] Schoenlein R W *et al.* 2000 *Science* **287** 2237
[10] Ackermann W *et al.* 2007 *Nature Phot.* **1** 336
[11] Emma P *et al.* 2010 *Nature Phot.* **4** 641
[12] Pile D *Nature Phot.* **5** 456
[13] Frasinski, L J *et al.* 2013 *Phys. Rev. Lett.* **111**, 073002
[14] Zhaunerchyk V *et al.* 2013 *J. Phys. B: At. Mol. Opt. Phys.* **46** 164034
[15] Rohringer N *et al.* 2012 *Nature* **481** 488
[16] Young L *et al.* 2010 *Nature* **466** 56
[17] Hoener M *et al.* 2010 Phys. Rev. Lett. **104** 253002
[18] Emma P *et al.* 2004 *Phys. Rev. Lett.* **92** 074801
[19] Mucke M., Zhaunerchyk, R.J. Squibb,..., and R. Feifel 2013 in preparation
[20] Schreier W *et al.* 2007 *Science* **315** 625
[21] Middleton C T *et al.* 2009 *Ann. Rev. Phys. Chem.* **60** 217
[22] Bozek J 2009 *Eur. Phys. J.* **169** 129
[23] Abdoul-Carime H *et al.* 2004 *Chem. Phys. Lett.* **387** 267
[24] Ullrich S, Schultz T, Zgierski M Z and Stolow, A 2004 *Phys. Chem. Chem. Phys.* **6**, 2796
[25] Ferro D, Bencivenni L, Teghil R, and Mastromarino R 1980 *Thermochim. Acta* **42** 75
[26] Moeller S *et al.* 2011 *Nucl. Instr. Meth. Phys. Res. A* **635** S6
[27] Hau-Riege S *et al.* 2008 *J. Appl. Phys.* **103** 053306
[28] Schorb S *et al.* 2012 *Appl. Phys. Lett.* **100**, 121107
[29] Trofimov A B, Schirmer J, Koychev J B, Potts A W, Holland D M P, and Karlsson L 2006 J. Phys. B. **39** 3005
[30] McFarland B K *et al.* 2013 submitted